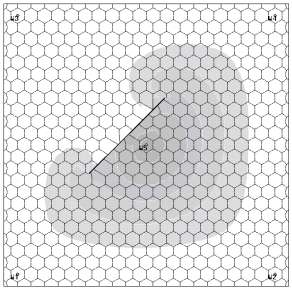

Chapter 9
The Compositional Model

Recall that to recover some of the hydrocarbons after water flooding, several enhanced recovery techniques are used. These involve complex chemical and thermal effects and are termed *tertiary recovery* or *enhanced recovery*. There are many different variations of enhanced recovery techniques. One of the main objectives of these techniques is to achieve miscibility and thus eliminate residual oil saturation. Miscibility can be achieved by increasing temperature (e.g., in situ combustion) or by injecting other chemical species such as CO_2. A typical flow in enhanced recovery is the *compositional flow*, where only the number of chemical species is a priori given, and the number of phases and the composition of each phase in terms of the given species depend on the thermodynamic conditions and the overall concentration of each species.

The governing equations for the compositional model are stated in Section 9.1. The Peng–Robinson equation of state is also briefly reviewed there. The iterative IMPES solution technique developed for the black oil model in Chapter 8 is further studied for the compositional model in Section 9.2. In Section 9.3, the solution of equilibrium relations that describe the mass distribution of chemical species among the fluid phases is discussed in detail. Numerical results based on the third CSP organized by the SPE are reported in Section 9.4. Finally, bibliographical information is given in Section 9.5.

9.1 Basic Differential Equations

9.1.1 The basic equations

The basic equations for the compositional model in a porous medium Ω were described in Section 2.8. For completeness, we review these equations. We describe a compositional model under the assumptions that the flow process is isothermal (i.e., constant temperature), the components form at most three phases (e.g., water, oil, and gas), there is no mass interchange between the water phase and the hydrocarbon phases (i.e., the oil and gas phases), and diffusive effects are neglected.

Let ϕ and $\mathbf{k}$ denote the porosity and permeability of the porous medium $\Omega \subset \mathbb{R}^3$, and let S_α, μ_α, p_α, $\mathbf{u}_\alpha$, and $k_{r\alpha}$ be the saturation, viscosity, pressure, volumetric velocity,

and relative permeability, respectively, of the α-phase, $\alpha = w, o, g$. Also, let ξ_{io} and ξ_{ig} represent the molar densities of component i in the oil (liquid) and gas (vapor) phases, respectively, $i = 1, 2, \ldots, N_c$, where N_c is the number of components. The molar density of phase α is given by

$$\xi_\alpha = \sum_{i=1}^{N_c} \xi_{i\alpha}, \qquad \alpha = o,\ g. \tag{9.1}$$

The mole fraction of component i in phase α is then

$$x_{i\alpha} = \xi_{i\alpha}/\xi_\alpha, \qquad i = 1, 2, \ldots, N_c,\ \alpha = o, g. \tag{9.2}$$

The total mass is conserved for each component:

$$\begin{aligned} &\frac{\partial(\phi\xi_w S_w)}{\partial t} + \nabla\cdot(\xi_w \mathbf{u}_w) = q_w, \\ &\frac{\partial(\phi[x_{io}\xi_o S_o + x_{ig}\xi_g S_g])}{\partial t} + \nabla\cdot(x_{io}\xi_o\mathbf{u}_o + x_{ig}\xi_g\mathbf{u}_g) \\ &\qquad = x_{io}q_o + x_{ig}q_g, \qquad i = 1, 2, \ldots, N_c, \end{aligned} \tag{9.3}$$

where ξ_w is the molar density of water (that is the water mass density ρ_w for the present model) and q_α stands for the flow rate of phase α at wells. In (9.3), the volumetric velocity $\mathbf{u}_\alpha$ is given by Darcy's law:

$$\mathbf{u}_\alpha = -\frac{k_{r\alpha}}{\mu_\alpha}\mathbf{k}\left(\nabla p_\alpha - \rho_\alpha \wp \nabla z\right), \qquad \alpha = w,\ o,\ g, \tag{9.4}$$

where ρ_α is the mass density of the α-phase, $\wp$ is the magnitude of the gravitational acceleration, and z is the depth. The mass density ρ_α is related to the molar density ξ_w by (2.93). The fluid viscosity $\mu_\alpha(p_\alpha, T, x_{1\alpha}, x_{2\alpha}, \ldots, x_{N_c\alpha})$ can be calculated from pressure, temperature, and compositions (Lohrenz et al., 1964).

In addition to the differential equations (9.3) and (9.4), there are also algebraic constraints. The mole fraction balance implies that

$$\sum_{i=1}^{N_c} x_{io} = 1, \quad \sum_{i=1}^{N_c} x_{ig} = 1. \tag{9.5}$$

In the transport process, the saturation constraint reads

$$S_w + S_o + S_g = 1. \tag{9.6}$$

Finally, the phase pressures are related by capillary pressures:

$$p_{cow} = p_o - p_w, \quad p_{cgo} = p_g - p_o. \tag{9.7}$$

Mass interchange between phases is characterized by the variation of mass distribution of each component in the oil and gas phases. As usual, these two phases are assumed to be in the phase equilibrium state at every moment. This is physically reasonable since mass interchange between phases occurs much faster than the flow of porous media fluids. Consequently, the distribution of each hydrocarbon component into the two phases is subject to the condition of *stable thermodynamic equilibrium*, which is given by minimizing the Gibbs free energy of the compositional system (Bear, 1972; Chen et al., 2000):

$$f_{io}(p_o, x_{1o}, x_{2o}, \ldots, x_{N_c o}) = f_{ig}(p_g, x_{1g}, x_{2g}, \ldots, x_{N_c g}), \tag{9.8}$$

where f_{io} and f_{ig} are the fugacity functions of the ith component in the oil and gas phases, respectively, $i = 1, 2, \ldots, N_c$.

Equations (9.3)–(9.8) provide $2N_c+9$ independent relations, differential or algebraic, for the $2N_c+9$ dependent variables: $x_{io}, x_{ig}, \mathbf{u}_\alpha, p_\alpha$, and $S_\alpha, \alpha = w, o, g, i = 1, 2, \ldots, N_c$. With appropriate boundary and initial conditions, this is a closed differential system for these unknowns.

9.1.2 Equations of state

The rock properties reviewed in Section 8.1.2 for the black oil model also apply to the compositional model. In particular, for convenience of programming, we define

$$p_{cw} = p_w - p_o, \quad p_{cg} = p_g - p_o; \tag{9.9}$$

i.e., $p_{cw} = -p_{cow}$ and $p_{cg} = p_{cgo}$. Moreover, for notational convenience, let $p_{co} = 0$.

Several equations of state (EOSs) were introduced in Section 3.2.5 for the definition of the fugacity functions f_{io} and f_{ig}, including the Redlich–Kwong, Redlich–Kwong–Soave, and Peng–Robinson EOSs. Here we briefly review the most frequently used Peng–Robinson EOS (Peng and Robinson, 1976; Coats, 1980).

The mixing principle for the Peng–Robinson equation of state is

$$\begin{aligned} a_\alpha &= \sum_{i=1}^{N_c}\sum_{j=1}^{N_c} x_{i\alpha}x_{j\alpha}(1-\kappa_{ij})\sqrt{a_i a_j}, \\ b_\alpha &= \sum_{i=1}^{N_c} x_{i\alpha} b_i, \qquad \alpha = o, g, \end{aligned}$$

where κ_{ij} is a *binary interaction* parameter between components i and j, and a_i and b_i are empirical factors for the pure component i. The interaction parameters account for molecular interactions between two unlike molecules. By definition, κ_{ij} is zero when i and j represent the same component, small when i and j represent components that do not differ much (e.g., when components i and j are both alkanes), and large when i and j represent components that are substantially different. Ideally, κ_{ij} depends on pressure and

temperature and only on the identities of components i and j (Zudkevitch and Joffe, 1970; Whitson, 1982).

The factors a_i and b_i can be computed from

$$a_i = \Omega_{ia}\alpha_i \frac{R^2 T_{ic}^2}{p_{ic}}, \quad b_i = \Omega_{ib}\frac{R\,T_{ic}}{p_{ic}},$$

where R is the universal gas constant, T is the temperature, T_{ic} and p_{ic} are the critical temperature and pressure, the EOS parameters Ω_{ia} and Ω_{ib} are given by

$$\begin{aligned}
&\Omega_{ia} = 0.45724, \quad \Omega_{ib} = 0.077796,\\
&\alpha_i = \left(1 - \lambda_i\left[1 - \sqrt{T/T_{ic}}\right]\right)^2,\\
&\lambda_i = 0.37464 + 1.5423\omega_i - 0.26992\omega_i^2,
\end{aligned}$$

and ω_i is the *acentric factor* for components i. The acentric factors roughly express the deviation of the shape of a molecule from a sphere (Reid et al., 1977). Define

$$A_\alpha = \frac{a_\alpha p_\alpha}{R^2 T^2}, \quad B_\alpha = \frac{b_\alpha p_\alpha}{R\,T}, \quad \alpha = o, g, \tag{9.10}$$

where the pressure p_α is given by the Peng–Robinson two-parameter EOS

$$p_\alpha = \frac{RT}{V_\alpha - b_\alpha} - \frac{a_\alpha(T)}{V_\alpha(V_\alpha + b_\alpha) + b_\alpha(V_\alpha - b_\alpha)} \tag{9.11}$$

with V_α being the molar volume of phase α. Introduce the compressibility factor

$$Z_\alpha = \frac{p_\alpha V_\alpha}{R\,T}, \qquad \alpha = o, g. \tag{9.12}$$

Equation (9.11) can be expressed as a cubic equation in Z_α:

$$\begin{aligned}
Z_\alpha^3 - (1 - B_\alpha)Z_\alpha^2 + (A_\alpha - 2B_\alpha - 3B_\alpha^2)Z_\alpha\\
- (A_\alpha B_\alpha - B_\alpha^2 - B_\alpha^3) = 0.
\end{aligned} \tag{9.13}$$

The correct choice of the root of (9.13) will be discussed in Section 9.3.4. Now, for $i = 1, 2, \ldots, N_c$ and $\alpha = o, g$, the fugacity coefficient $\varphi_{i\alpha}$ of component i in the mixture can be obtained from

$$\begin{aligned}
\ln\varphi_{i\alpha} = {} & \frac{b_i}{b_\alpha}(Z_\alpha - 1) - \ln(Z_\alpha - B_\alpha)\\
& - \frac{A_\alpha}{2\sqrt{2}B_\alpha}\left(\frac{2}{a_\alpha}\sum_{j=1}^{N_c} x_{j\alpha}(1 - \kappa_{ij})\sqrt{a_i a_j} - \frac{b_i}{b_\alpha}\right)\\
& \cdot \ln\left(\frac{Z_\alpha + (1 + \sqrt{2})B_\alpha}{Z_\alpha - (1 - \sqrt{2})B_\alpha}\right).
\end{aligned} \tag{9.14}$$

Finally, the fugacity of component i is

$$f_{i\alpha} = p_\alpha x_{i\alpha} \varphi_{i\alpha}, \qquad i = 1, 2, \ldots, N_c, \ \alpha = o, g. \tag{9.15}$$

The mass distribution of each hydrocarbon component into the fluid (oil) and vapor (gas) phases is given by the thermodynamic equilibrium relation (9.8).

9.2 Solution Techniques

The choice of a solution technique is crucial for a coupled system of partial differential equations. In the preceding chapter, we discussed several solution techniques that are currently used in the numerical solution of the black oil model. These techniques include the iterative IMPES, sequential, SS, and adaptive implicit techniques. They can be also employed for the numerical simulation of the compositional model. However, a typical compositional simulator includes about a dozen chemical components; the SS would be a very expensive technique for this type of flow, even with today's computing power. The iterative IMPES and sequential techniques are widely used and are thus studied here. As an example, we develop iterative IMPES for the compositional model. An extension from this technique to the sequential technique can be carried out as in the preceding chapter for the black oil model.

9.2.1 Choice of primary variables

Equations (9.3)–(9.8) form a strongly coupled system of time-dependent, nonlinear differential equations and algebraic constraints. While there are $2N_c + 9$ equations for the same number of dependent variables, this system can be written in terms of $2N_c + 2$ primary variables, and other variables can be expressed as functions of them. These primary variables must be carefully chosen so that the main physical properties inherent in the governing equations and constraints are preserved, the nonlinearity and coupling between the equations is weakened, and efficient numerical methods for the solution of the resulting system can be devised.

To simplify the expressions in (9.3), we introduce the potentials

$$\Phi_\alpha = p_\alpha - \rho_\alpha \wp z, \qquad \alpha = w, o, g. \tag{9.16}$$

Also, we use the *total mass variable* F of the hydrocarbon system (Nolen, 1973; Young and Stephenson, 1983)

$$F = \xi_o S_o + \xi_g S_g, \tag{9.17}$$

and the *mass fractions* of oil and gas in this system,

$$L = \frac{\xi_o S_o}{F}, \quad V = \frac{\xi_g S_g}{F}. \tag{9.18}$$

Note that

$$L + V = 1.$$

Next, instead of exploiting the individual mole fractions, we use the *total mole fraction* of the components in the hydrocarbon system

$$z_i = Lx_{io} + (1 - L)x_{ig}, \qquad i = 1, 2, \ldots, N_c. \tag{9.19}$$

Then we see, using (9.5), (9.17), and (9.18), that

$$\sum_{i=1}^{N_c} z_i = 1 \tag{9.20}$$

and

$$x_{io}\xi_o S_o + x_{ig}\xi_g S_g = F z_i, \qquad i = 1, 2, \ldots, N_c. \tag{9.21}$$

Consequently, applying (9.4) and (9.16), the second equation in (9.3) becomes (cf. Exercise 9.1)

$$\begin{aligned} \frac{\partial(\phi F z_i)}{\partial t} - \nabla \cdot \left(\mathbf{k} \left[\frac{x_{io}\xi_o k_{ro}}{\mu_o} \nabla \Phi_o + \frac{x_{ig}\xi_g k_{rg}}{\mu_g} \nabla \Phi_g \right] \right) \\ = x_{io} q_o + x_{ig} q_g, \qquad i = 1, 2, \ldots, N_c. \end{aligned} \tag{9.22}$$

Adding equations (9.22) over i and exploiting (9.5) and (9.20) gives

$$\frac{\partial(\phi F)}{\partial t} - \nabla \cdot \left(\mathbf{k} \left[\frac{\xi_o k_{ro}}{\mu_o} \nabla \Phi_o + \frac{\xi_g k_{rg}}{\mu_g} \nabla \Phi_g \right] \right) = q_o + q_g. \tag{9.23}$$

Equation (9.22) is the individual flow equation for the ith component (say, $i = 1, 2, \ldots, N_c - 1$) and (9.23) is the global hydrocarbon flow equation.

To simplify the differential equations further, we define the transmissibilities

$$\begin{aligned} \mathbf{T}_\alpha &= \frac{\xi_\alpha k_{r\alpha}}{\mu_\alpha} \mathbf{k}, && \alpha = w, o, g, \\ \mathbf{T}_{i\alpha} &= \frac{x_{i\alpha}\xi_\alpha k_{r\alpha}}{\mu_\alpha} \mathbf{k}, && \alpha = o, g, \ i = 1, 2, \ldots, N_c. \end{aligned} \tag{9.24}$$

We now summarize the equations needed in iterative IMPES. The equilibrium relation (9.8) is recast as

$$\begin{aligned} f_{io}(p_o, x_{1o}, x_{2o}, \ldots, x_{N_c o}) = f_{ig}(p_o + p_{cg}, x_{1g}, x_{2g}, \ldots, x_{N_c g}), \\ i = 1, 2, \ldots, N_c. \end{aligned} \tag{9.25}$$

Using (9.24), equation (9.22) becomes

$$\begin{aligned} \frac{\partial(\phi F z_i)}{\partial t} = \nabla \cdot (\mathbf{T}_{io} \nabla \Phi_o + \mathbf{T}_{ig} \nabla \Phi_g) + x_{io} q_o + x_{ig} q_g, \\ i = 1, 2, \ldots, N_c - 1. \end{aligned} \tag{9.26}$$

Similarly, it follows from (9.23) that

$$\frac{\partial(\phi F)}{\partial t} = \nabla \cdot (\mathbf{T}_o \nabla \Phi_o + \mathbf{T}_g \nabla \Phi_g) + q_o + q_g. \tag{9.27}$$

Next, applying the first equation of (9.3) and (9.24) yields

$$\frac{\partial(\phi\xi_w S_w)}{\partial t} = \nabla\cdot(\mathbf{T}_w\nabla\Phi_w) + q_w. \tag{9.28}$$

Finally, using (9.17) and (9.18), the saturation state equation (9.6) becomes

$$F\left(\frac{L}{\xi_o} + \frac{1-L}{\xi_g}\right) + S = 1. \tag{9.29}$$

The differential system consists of the $2N_c + 2$ equations (9.25)–(9.29) for the $2N_c + 2$ primary unknowns: x_{io} (or x_{ig}), L (or V), z_i, F, $S = S_w$, and $p = p_o$, $i = 1, 2, \ldots, N_c - 1$.

9.2.2 Iterative IMPES

Let $n > 0$ (an integer) indicate a time step. For any function v of time, we use $\bar{\delta}v$ to denote the time increment at the nth step:

$$\bar{\delta}v = v^{n+1} - v^n.$$

A time approximation at the $(n+1)$th level for the system of equations (9.25)–(9.29) is

$$\begin{aligned}
&f_{io}(p_o^{n+1}, x_{1o}^{n+1}, x_{2o}^{n+1}, \ldots, x_{N_co}^{n+1})\\
&\quad = f_{ig}(p_g^{n+1}, x_{1g}^{n+1}, x_{2g}^{n+1}, \ldots, x_{N_cg}^{n+1}), \qquad i = 1, 2, \ldots, N_c,\\
&\frac{1}{\Delta t}\bar{\delta}(\phi F z_i) = \nabla\cdot(\mathbf{T}_{io}^n\nabla\Phi_o^{n+1} + \mathbf{T}_{ig}^n\nabla\Phi_g^{n+1})\\
&\qquad\qquad + x_{io}^{n+1}q_o^n + x_{ig}^{n+1}q_g^n, \qquad i = 1, 2, \ldots, N_c - 1,\\
&\frac{1}{\Delta t}\bar{\delta}(\phi F) = \nabla\cdot(\mathbf{T}_o^n\nabla\Phi_o^{n+1} + \mathbf{T}_g^n\nabla\Phi_g^{n+1}) + q_o^n + q_g^n,\\
&\frac{1}{\Delta t}\bar{\delta}(\phi\xi_w S) = \nabla\cdot(\mathbf{T}_w^n\nabla\Phi_w^{n+1}) + q_w^n,\\
&\left[F\left(\frac{L}{\xi_o} + \frac{1-L}{\xi_g}\right) + S\right]^{n+1} = 1,
\end{aligned} \tag{9.30}$$

where $\Delta t = t^{n+1} - t^n$. Note that the transmissibilities and well terms in (9.30) are evaluated at the previous time level.

System (9.30) is nonlinear in the primary unknowns, and can be linearized via the Newton–Raphson iteration introduced in Section 8.2.1. For a generic function v of time, we use the iteration

$$v^{n+1,l+1} = v^{n+1,l} + \delta v,$$

where l refers to the iteration number of Newton–Raphson's iterations and δv represents the

increment in this iteration step. When no ambiguity occurs, we will replace $v^{n+1,l+1}$ and $v^{n+1,l}$ by v^{l+1} and v^l, respectively (i.e., the superscript $n+1$ is omitted). Observe that

$$v^{n+1} \approx v^{l+1} = v^l + \delta v,$$

so

$$\bar{\delta} v \approx v^l - v^n + \delta v.$$

Using this approximation in system (9.30) gives

$$\begin{aligned}
&f_{io}(p_o^{l+1}, x_{1o}^{l+1}, x_{2o}^{l+1}, \ldots, x_{N_c o}^{l+1}) \\
&\quad = f_{ig}(p_g^{l+1}, x_{1g}^{l+1}, x_{2g}^{l+1}, \ldots, x_{N_c g}^{l+1}), \qquad i = 1, 2, \ldots, N_c, \\
&\frac{1}{\Delta t}\left[(\phi F z_i)^l - (\phi F z_i)^n + \delta(\phi F z_i)\right] \\
&\quad = \nabla \cdot (\mathbf{T}_{io}^n \nabla \Phi_o^{l+1} + \mathbf{T}_{ig}^n \nabla \Phi_g^{l+1}) + x_{io}^{l+1} q_o^n + x_{ig}^{l+1} q_g^n, \\
&\qquad\qquad i = 1, 2, \ldots, N_c - 1, \\
&\frac{1}{\Delta t}\left[(\phi F)^l - (\phi F)^n + \delta(\phi F)\right] \\
&\quad = \nabla \cdot (\mathbf{T}_o^n \nabla \Phi_o^{l+1} + \mathbf{T}_g^n \nabla \Phi_g^{l+1}) + q_o^n + q_g^n, \\
&\frac{1}{\Delta t}\left[(\phi \xi_w S)^l - (\phi \xi_w S)^n + \delta(\phi \xi_w S)\right] = \nabla \cdot (\mathbf{T}_w^n \nabla \Phi_w^{l+1}) + q_w^n, \\
&\left[F\left(\frac{L}{\xi_o} + \frac{1-L}{\xi_g}\right) + S\right]^{l+1} = 1.
\end{aligned} \tag{9.31}$$

We expand the potentials and transmissibilities in terms of the primary unknowns. Toward that end, we must identify these unknowns. If the gas phase dominates in the hydrocarbon system (e.g., $L < 0.5$), the primary unknowns will be x_{io}, L, z_i, F, S, and p, $i = 1, 2, \ldots, N_c - 1$, which is the $L - X$ *iteration type* in compositional modeling. If the oil phase dominates (e.g., $L \geq 0.5$), the primary unknowns will be x_{ig}, V, z_i, F, S, and p, $i = 1, 2, \ldots, N_c - 1$, which corresponds to the $V - Y$ *iteration type*. As an example, we illustrate how to expand the potentials and transmissibilities in terms of δx_{io}, δL, δz_i, δF, δS, and δp, $i = 1, 2, \ldots, N_c - 1$; a similar expansion can be performed for the $V - Y$ iteration type.

For the ith component flow equation,

$$\delta(\phi F z_i) = c_{ip}\delta p + c_{iF}\delta F + c_{iz}\delta z_i, \qquad i = 1, 2, \ldots, N_c - 1, \tag{9.32}$$

where

$$c_{ip} = \phi^o c_R (F z_i)^l, \quad c_{iF} = (\phi z_i)^l, \quad c_{iz} = (\phi F)^l,$$

with ϕ^o being the porosity at a reference pressure p^o and c_R the rock compressibility. For the global hydrocarbon flow equation,

$$\delta(\phi F) = c_p \delta p + c_F \delta F, \tag{9.33}$$

where

$$c_p = \phi^o c_R F^l, \quad c_F = \phi^l.$$

For the water flow equation,

$$\delta(\phi \xi_w S) = c_{wp} \delta p + c_{wS} \delta S, \tag{9.34}$$

where

$$c_{wp} = \phi^o c_R (\xi_w S)^l + \left(\phi \frac{d\xi_w}{dp} S\right)^l, \quad c_{wS} = (\phi \xi_w)^l.$$

In iterative IMPES, all the saturation functions (k_{rw}, k_{ro}, k_{rg}, p_{cw}, and p_{cg}), densities, and viscosities are evaluated at the saturation values of the previous time step in the Newton–Raphson iteration. The phase potentials are calculated by

$$\Phi_\alpha^{l+1} = p^{l+1} + p_{c\alpha}^n - \rho_\alpha^n \wp z, \qquad \alpha = w, o, g, \tag{9.35}$$

and the transmissibilities by

$$\begin{aligned} \mathbf{T}_\alpha^n &= \frac{\xi_\alpha^n k_{r\alpha}^n}{\mu_\alpha^n} \mathbf{k}, && \alpha = w, o, g, \\ \mathbf{T}_{i\alpha}^n &= \frac{x_{i\alpha}^n \xi_\alpha^n k_{r\alpha}^n}{\mu_\alpha^n} \mathbf{k}, && \alpha = o, g, \ i = 1, 2, \ldots, N_c. \end{aligned} \tag{9.36}$$

It follows from (9.35) that

$$\Phi_\alpha^{l+1} = \Phi_\alpha^l + \delta p, \qquad \alpha = w, o, g. \tag{9.37}$$

We now expand each of the equations in system (9.31). For this, we replace the derivatives in x_{ig} by those in the primary variables, $i = 1, 2, \ldots, N_c$. Applying relation (9.19), we see that

$$\begin{aligned} &\frac{\partial x_{ig}}{\partial x_{io}} = \frac{L}{L-1}, \qquad \frac{\partial x_{ig}}{\partial z_i} = \frac{1}{1-L}, \\ &\frac{\partial x_{ig}}{\partial L} = \frac{x_{io} - x_{ig}}{L-1}, \qquad i = 1, 2, \ldots, N_c. \end{aligned}$$

Consequently, the chain rule implies

$$\begin{aligned} \frac{\partial}{\partial x_{io}} &= \frac{\partial x_{ig}}{\partial x_{io}} \frac{\partial}{\partial x_{ig}} = \frac{L}{L-1} \frac{\partial}{\partial x_{ig}}, \\ \frac{\partial}{\partial z_i} &= \frac{\partial x_{ig}}{\partial z_i} \frac{\partial}{\partial x_{ig}} = \frac{1}{1-L} \frac{\partial}{\partial x_{ig}}, \\ \frac{\partial}{\partial L} &= \frac{\partial x_{ig}}{\partial L} \frac{\partial}{\partial x_{ig}} = \frac{x_{io} - x_{ig}}{L-1} \frac{\partial}{\partial x_{ig}}. \end{aligned}$$

Thus, after using (9.5) and (9.20) to eliminate $x_{N_c o}$ and z_{N_c}, the first equation in (9.31) can be expanded:

$$\begin{aligned}
&\sum_{j=1}^{N_c-1}\left\{\left(\frac{\partial f_{io}}{\partial x_{jo}}\right)^l-\left(\frac{\partial f_{io}}{\partial x_{N_c o}}\right)^l+\frac{L^l}{1-L^l}\left[\left(\frac{\partial f_{ig}}{\partial x_{jg}}\right)^l-\left(\frac{\partial f_{ig}}{\partial x_{N_c g}}\right)^l\right]\right\}\delta x_{jo}\\
&\quad+\frac{1}{1-L^l}\sum_{j=1}^{N_c}\left(\frac{\partial f_{ig}}{\partial x_{jg}}\left(x_{jo}-x_{jg}\right)\right)^l\delta L\\
&=f_{ig}^l-f_{io}^l+\left[\left(\frac{\partial f_{ig}}{\partial p}\right)^l-\left(\frac{\partial f_{io}}{\partial p}\right)^l\right]\delta p\\
&\quad+\frac{1}{1-L^l}\sum_{j=1}^{N_c-1}\left[\left(\frac{\partial f_{ig}}{\partial x_{jg}}\right)^l-\left(\frac{\partial f_{ig}}{\partial x_{N_c g}}\right)^l\right]\delta z_j,
\end{aligned}\tag{9.38}$$

where, for $i=1,2,\ldots,N_c$,

$$f_{io}^l=f_{io}(p_o^l,x_{1o}^l,x_{2o}^l,\ldots,x_{N_c o}^l),\qquad f_{ig}^l=f_{ig}(p_g^l,x_{1g}^l,x_{2g}^l,\ldots,x_{N_c g}^l).$$

The linear equation (9.38) is used to solve for $(\delta x_{1o},\delta x_{2o},\ldots,\delta x_{(N_c-1)o},\delta L)$ in terms of $(\delta z_1,\delta z_2,\ldots,\delta z_{N_c-1},\delta p)$.

Next, applying (9.32) and (9.37), from the second equation in (9.31) it follows that, for $i=1,2,\ldots,N_c-1$,

$$\begin{aligned}
&\frac{1}{\Delta t}\left[(\phi F z_i)^l-(\phi F z_i)^n+c_{ip}\delta p+c_{iF}\delta F+c_{iz}\delta z_i\right]\\
&\quad=\nabla\cdot(\mathbf{T}_{io}^n\nabla\Phi_o^l+\mathbf{T}_{ig}^n\nabla\Phi_g^l)+\nabla\cdot\Big((\mathbf{T}_{io}^n+\mathbf{T}_{ig}^n)\nabla(\delta p)\Big)\\
&\qquad+\left(x_{io}^l+\delta x_{io}\right)q_o(\delta p)+\Big(x_{ig}^l+\delta x_{ig}\Big)q_g(\delta p).
\end{aligned}\tag{9.39}$$

Equation (9.39) is solved for $(\delta z_1,\delta z_2,\ldots,\delta z_{N_c-1})$ in terms of $(\delta F,\delta p)$. Similarly, from the third equation in (9.31) we see that

$$\begin{aligned}
&\frac{1}{\Delta t}\left[(\phi F)^l-(\phi F)^n+c_p\delta p+c_F\delta F\right]\\
&\quad=\nabla\cdot(\mathbf{T}_o^n\nabla\Phi_o^l+\mathbf{T}_g^n\nabla\Phi_g^l)+\nabla\cdot\Big((\mathbf{T}_o^n+\mathbf{T}_g^n)\nabla(\delta p)\Big)\\
&\qquad+q_o(\delta p)+q_g(\delta p),
\end{aligned}\tag{9.40}$$

which gives δF in terms of δp. From the fourth equation in (9.31), (9.34), and (9.37), we have

$$\begin{aligned}&\frac{1}{\Delta t}\left[(\phi\xi_w S)^l-(\phi\xi_w S)^n+c_{wp}\delta p+c_{wS}\delta S\right]\\&\quad=\nabla\cdot(\mathbf{T}_w^n\nabla\Phi_w^l)+\nabla\cdot\left(\mathbf{T}_w^n\nabla(\delta p)\right)+q_w(\delta p).\end{aligned}\tag{9.41}$$

Equation (9.41) gives δS in terms of δp.

It follows from (9.12) that

$$\frac{1}{\xi_\alpha}=\frac{Z_\alpha(p_\alpha,x_{1\alpha},x_{2\alpha},\ldots,x_{N_c\alpha})R\,T}{p_\alpha},\qquad \alpha=o,g.$$

Applying (9.5) and (9.20), it follows from the last equation in (9.31) that

$$\begin{aligned}&\left(\frac{FLRT}{p}\right)^l\sum_{j=1}^{N_c-1}\left\{\left(\frac{\partial Z_o}{\partial x_{jo}}\right)^l-\left(\frac{\partial Z_o}{\partial x_{N_co}}\right)^l\right.\\&\qquad\left.-\left[\left(\frac{\partial Z_g}{\partial x_{jg}}\right)^l-\left(\frac{\partial Z_g}{\partial x_{N_cg}}\right)^l\right]\right\}\delta x_{jo}\\&+\left(\frac{FRT}{p}\right)^l\left[Z_o-Z_g-\sum_{j=1}^{N_c}\left(\frac{\partial Z_g}{\partial x_{jg}}\left(x_{jo}-x_{jg}\right)\right)^l\right]\delta L\\&+\left(\frac{FRT}{p}\right)^l\sum_{j=1}^{N_c-1}\left\{\left(\frac{\partial Z_g}{\partial x_{jg}}\right)^l-\left(\frac{\partial Z_g}{\partial x_{N_cg}}\right)^l\right\}\delta z_j\\&+\left(\frac{RT}{p}\left(LZ_o+(1-L)Z_g\right)\right)^l\delta F+\delta S\\&+\left(\frac{FRT}{p}\left[L\frac{\partial Z_o}{\partial p}-\frac{LZ_o}{p}+(1-L)\frac{\partial Z_g}{\partial p}-\frac{(1-L)Z_g}{p}\right]\right)^l\delta p\\&=1-\left(F\left[\frac{L}{\xi_o}+\frac{1-L}{\xi_g}\right]+S\right)^l.\end{aligned}\tag{9.42}$$

After substituting δx_{jo}, δL, δz_j, δF, and δS, $j=1,2,\ldots,N_c-1$, into (9.42) using (9.38)–(9.41), the resulting equation becomes the pressure equation, which, together with the well control equations (cf. Chapter 8), is implicitly solved for δp. After δp is obtained, (9.41), (9.40), (9.39), and (9.38) are solved explicitly for δS, δF, $(\delta z_1,\delta z_2,\ldots,\delta z_{N_c-1})$, and $(\delta x_{1o},\delta x_{2o},\ldots,\delta x_{(N_c-1)o},\delta L)$, respectively. The numerical methods introduced in Chapter 4 can be applied to the discretization of (9.38)–(9.42) in space.

In summary, the iterative IMPES for the compositional model has following features:

- The difference between iterative IMPES and classical IMPES is that the iterative one is used within each Newton–Raphson iteration loop, while the classical one is utilized outside the Newton–Raphson iteration.

- The saturation constraint equation is used to solve implicitly for pressure p.
- The equilibrium relation is solved for $(x_{1o}, x_{2o}, \ldots, x_{(N_c-1)o}, L)$.
- The hydrocarbon component flow equations are used to obtain $(z_1, z_2, \ldots, z_{N_c-1})$ explicitly.
- The global hydrocarbon flow equation is exploited to solve explicitly for F.
- The water flow equation is explicitly solved for S.
- Relation (9.19) generates $(x_{1g}, x_{2g}, \ldots, x_{N_c g})$.

As in the sequential technique for the black oil model, the saturation functions k_{rw}, k_{ro}, k_{rg}, p_{cw}, and p_{cg} can use the previous Newton–Raphson iteration values of saturations, instead of the previous time step values of saturations.

9.3 Solution of Equilibrium Relations

We discuss the solution of the thermodynamic equilibrium relation (9.25), which describes the mass distribution of each component in the oil and gas phases. As an example, we concentrate on the Peng–Robinson equation of state.

9.3.1 Successive substitution method

The *successive substitution method* is often employed to find an initial guess for the computation of the thermodynamic equilibrium relation (9.38) in the Newton–Raphson flash calculation discussed in the next subsection. The *equilibrium flash vaporization ratio* for component i is defined by

$$K_i = \frac{x_{ig}}{x_{io}}, \qquad i = 1, 2, \ldots, N_c, \tag{9.43}$$

where the quantity K_i is the K-value of component i. If the iterative IMPES in the previous section is used (i.e., the capillary pressure p_{cg} is evaluated at the previous time step value of saturations in the Newton–Raphson iteration), it follows from (9.15) that

$$f_{i\alpha} = p x_{i\alpha} \varphi_{i\alpha}, \qquad i = 1, 2, \ldots, N_c, \ \alpha = o, g. \tag{9.44}$$

Then, using (9.8), we see that

$$x_{io}\varphi_{io} = x_{ig}\varphi_{ig}, \qquad i = 1, 2, \ldots, N_c.$$

Thus, by (9.43), we have

$$K_i = \frac{\varphi_{io}}{\varphi_{ig}}, \qquad i = 1, 2, \ldots, N_c, \tag{9.45}$$

where the fugacity coefficients φ_{io} and φ_{ig} are defined in (9.14).

A *flash calculation* is an instant phase equilibrium:

Given p, T, and z_i;
Find L (or V), x_{io}, and x_{ig}, $\qquad i = 1, 2, \ldots, N_c$.

It follows from (9.19) and (9.43) that

$$\begin{aligned} &x_{io} = \frac{z_i}{L + (1-L)K_i}, \qquad i = 1, 2, \ldots, N_c, \\ &\sum_{i=1}^{N_c} \frac{z_i(1-K_i)}{L + (1-L)K_i} = 0. \end{aligned} \tag{9.46}$$

Based on (9.46), we introduce the following successive substitution method for the flash calculation:

Initially, K_i is evaluated by the empirical formula

$$K_i = \frac{1}{p_{ir}} \exp\left(5.3727(1+\omega_i)\left[1 - \frac{1}{T_{ir}}\right]\right), \quad p_{ir} = \frac{p}{p_{ic}},\ T_{ir} = \frac{T}{T_{ic}};$$

(F1) Given K_i and z_i, find L by

$$\sum_{i=1}^{N_c} \frac{z_i(1-K_i)}{L + (1-L)K_i} = 0;$$

(F2) Find x_{io} and x_{ig} by

$$x_{io} = \frac{z_i}{L + (1-L)K_i}, \quad x_{ig} = K_i x_{io}, \quad i = 1, 2, \ldots, N_c;$$

(F3) Calculate K_i and z_i by

$$K_i = \frac{\varphi_{io}}{\varphi_{ig}}, \quad z_i = Lx_{io} + (1-L)x_{ig}, \quad i = 1, 2, \ldots, N_c;$$

Return to (F1) and iterate until the convergence of the values K_i.

In general, convergence of this successive substitution method is very slow. However, it can be used as an initialization for the Newton–Raphson flash iteration discussed below.

9.3.2 Newton–Raphson's flash calculation

Introduce the notation

$$G_{ij} = \left(\frac{\partial f_{io}}{\partial x_{jo}}\right)^l - \left(\frac{\partial f_{io}}{\partial x_{N_c o}}\right)^l + \frac{L^l}{1-L^l}\left[\left(\frac{\partial f_{ig}}{\partial x_{jg}}\right)^l - \left(\frac{\partial f_{ig}}{\partial x_{N_c g}}\right)^l\right],$$

$$G_{iN_c} = \frac{1}{1-L^l}\sum_{j=1}^{N_c}\left(\frac{\partial f_{ig}}{\partial x_{jg}}\left(x_{jo} - x_{jg}\right)\right)^l,$$

$$\begin{aligned} H_i(\delta p, \delta z_1, \delta z_2, \ldots, \delta z_{N_c-1}) = f_{ig}^l - f_{io}^l + &\left[\left(\frac{\partial f_{ig}}{\partial p}\right)^l - \left(\frac{\partial f_{io}}{\partial p}\right)^l\right]\delta p \\ &+ \frac{1}{1-L^l}\sum_{j=1}^{N_c-1}\left[\left(\frac{\partial f_{ig}}{\partial x_{jg}}\right)^l - \left(\frac{\partial f_{ig}}{\partial x_{N_c g}}\right)^l\right]\delta z_j \end{aligned}$$

for $i = 1, 2, \ldots, N_c$, $j = 1, 2, \ldots, N_c - 1$. Then (9.38) can be written in matrix form

$$\begin{pmatrix} G_{11} & G_{12} & \cdots & G_{1,N_c-1} & G_{1,N_c} \\ G_{21} & G_{22} & \cdots & G_{2,N_c-1} & G_{2,N_c} \\ \vdots & \vdots & \vdots & \vdots & \vdots \\ G_{N_c-1,1} & G_{N_c-1,2} & \cdots & G_{N_c-1,N_c-1} & G_{N_c-1,N_c} \\ G_{N_c,1} & G_{N_c,2} & \cdots & G_{N_c,N_c-1} & G_{N_c,N_c} \end{pmatrix} \begin{pmatrix} \delta x_{1o} \\ \delta x_{2o} \\ \vdots \\ \delta x_{(N_c-1)o} \\ \delta L \end{pmatrix} = \begin{pmatrix} H_1 \\ H_2 \\ \vdots \\ H_{N_c-1} \\ H_{N_c} \end{pmatrix}. \tag{9.47}$$

This system gives $(\delta x_{1o}, \delta x_{2o}, \ldots, \delta x_{(N_c-1)o}, \delta L)$ in terms of δz_i, $i = 1, 2, \ldots, N_c - 1$, and δp.

We point out the difference between the successive substitution method and the Newton–Raphson iteration in the flash calculation.

- The former method is easier to implement and is more reliable, even near a critical point. However, its convergence is usually slower; it may take over 1,000 iterations near the critical point.
- The latter method is faster. But it needs a good initial guess for x_{io} and L, $i = 1, 2, \ldots, N_c$; moreover, this method may not converge near a critical point.
- These two methods can be combined. For example, the former is used to find a good initial guess for the latter. Also, in places where the latter is difficult to converge, the former can be utilized instead.

9.3.3 Derivatives of fugacity coefficients

We calculate the partial derivatives involved in the Jacobian coefficient matrix of (9.47). First, by (9.44), for $i, j = 1, 2, \ldots, N_c$, $\alpha = o, g$,

$$\frac{\partial f_{i\alpha}}{\partial p} = x_{i\alpha}\varphi_{i\alpha} + p x_{i\alpha}\frac{\partial \varphi_{i\alpha}}{\partial p}, \quad \frac{\partial f_{i\alpha}}{\partial x_{j\alpha}} = p\frac{\partial x_{i\alpha}}{\partial x_{j\alpha}}\varphi_{i\alpha} + p x_{i\alpha}\frac{\partial \varphi_{i\alpha}}{\partial x_{j\alpha}},$$

where

$$\frac{\partial x_{i\alpha}}{\partial x_{j\alpha}} = \begin{cases} 1 & \text{if } i = j, \\ 0 & \text{if } i \neq j. \end{cases}$$

So it suffices to find the derivatives of $\varphi_{i\alpha}$, which is defined by (9.14), $i = 1, 2, \ldots, N_c$, $\alpha = o, g$.

It follows from (9.10) that

$$\frac{\partial A_\alpha}{\partial p} = \frac{a_\alpha}{R^2 T^2}, \quad \frac{\partial B_\alpha}{\partial p} = \frac{b_\alpha}{R\,T}, \quad \alpha = o, g. \tag{9.48}$$

Differentiating both sides of (9.14) gives

$$\begin{aligned}\frac{1}{\varphi_{i\alpha}}\frac{\partial\varphi_{i\alpha}}{\partial p} = \frac{b_i}{b_\alpha}\frac{\partial Z_\alpha}{\partial p} - \frac{1}{Z_\alpha - B_\alpha}\left(\frac{\partial Z_\alpha}{\partial p} - \frac{B_\alpha}{p}\right)\\ - \frac{A_\alpha}{2\sqrt{2}B_\alpha}\left(\frac{2}{a_\alpha}\sum_{j=1}^{N_c} x_{j\alpha}(1-\kappa_{ij})\sqrt{a_i a_j} - \frac{b_i}{b_\alpha}\right)\\ \cdot 2B_\alpha\left(\frac{Z_\alpha}{p} - \frac{\partial Z_\alpha}{\partial p}\right)\Bigg/\left(Z_\alpha^2 + 2\sqrt{2}Z_\alpha B_\alpha + B_\alpha^2\right).\end{aligned} \tag{9.49}$$

Similarly, we can obtain $\partial\varphi_{i\alpha}/\partial x_{j\alpha}$ using the expressions (cf. Exercise 9.2)

$$\begin{aligned}&\frac{\partial A_\alpha}{\partial x_{j\alpha}} = \frac{p}{R^2T^2}\frac{\partial a_\alpha}{\partial x_{j\alpha}}, \quad \frac{\partial B_\alpha}{\partial x_{j\alpha}} = \frac{p}{RT}\frac{\partial b_\alpha}{\partial x_{j\alpha}},\\ &\frac{\partial a_\alpha}{\partial x_{j\alpha}} = 2\sum_{i=1}^{N_c} x_{i\alpha}(1-\kappa_{ij})\sqrt{a_i a_j}, \quad \frac{\partial b_\alpha}{\partial x_{j\alpha}} = b_j\end{aligned} \tag{9.50}$$

for $i, j = 1, 2, \ldots, N_c$, $\alpha = o, g$.

The Z-factors, Z_α ($\alpha = o, g$), are determined by (9.13), which can be differentiated to find their derivatives. Implicit differentiation on (9.13) yields

$$\begin{aligned}\frac{\partial Z_\alpha}{\partial p} = -\Bigg\{\frac{\partial B_\alpha}{\partial p}Z_\alpha^2 + \left(\frac{\partial A_\alpha}{\partial p} - 2\left[1+3B_\alpha\right]\frac{\partial B_\alpha}{\partial p}\right)Z_\alpha\\ - \left(\frac{\partial A_\alpha}{\partial p}B_\alpha + \left[A_\alpha - 2B_\alpha - 3B_\alpha^2\right]\frac{\partial B_\alpha}{\partial p}\right)\Bigg\}\\ \Bigg/\left(2Z_\alpha^2 - 2(1-B_\alpha)Z_\alpha + (A_\alpha - 2B_\alpha - 3B_\alpha^2)\right).\end{aligned} \tag{9.51}$$

Consequently, substituting (9.48) into (9.51) gives $\partial Z_\alpha/\partial p$. A similar argument, together with (9.50), gives the derivatives $\partial Z_\alpha/\partial x_{j\alpha}$ (cf. Exercise 9.3), $j = 1, 2, \ldots, N_c$.

9.3.4 Solution of Peng–Robinson's cubic equation

The Peng–Robinson cubic equation (9.13) has the form

$$\mathcal{Z}^3 + B\mathcal{Z}^2 + C\mathcal{Z} + D = 0 \tag{9.52}$$

with given inputs B, C, and D. Before discussing the solution of this equation, we consider a simpler cubic equation:

$$X^3 + PX + Q = 0. \tag{9.53}$$

With

$$\Delta = \left(\frac{Q}{2}\right)^2 + \left(\frac{P}{3}\right)^3,$$

equation (9.53) has three roots (cf. Exercise 9.4)

$$\begin{aligned}
X_1 &= \sqrt[3]{-\frac{Q}{2} + \sqrt{\Delta}} + \sqrt[3]{-\frac{Q}{2} - \sqrt{\Delta}},\\
X_2 &= \omega\sqrt[3]{-\frac{Q}{2} + \sqrt{\Delta}} + \omega^2\sqrt[3]{-\frac{Q}{2} - \sqrt{\Delta}},\\
X_3 &= \omega^2\sqrt[3]{-\frac{Q}{2} + \sqrt{\Delta}} + \omega\sqrt[3]{-\frac{Q}{2} - \sqrt{\Delta}},
\end{aligned}$$

where

$$\omega = \frac{-1 + i\sqrt{3}}{2}, \quad \omega^2 = \frac{-1 - i\sqrt{3}}{2}, \quad i^2 = -1.$$

Note that (cf. Exercise 9.5)

$$X_1 + X_2 + X_3 = 0, \quad \frac{1}{X_1} + \frac{1}{X_2} + \frac{1}{X_3} = -\frac{P}{Q}, \quad X_1X_2X_3 = -Q. \tag{9.54}$$

If $\Delta > 0$, (9.53) has only one real root X_1. If $P = Q = 0$, there is solely the trivial solution $X_1 = X_2 = X_3 = 0$. When $\Delta \le 0$, there are three real roots given by

$$\begin{aligned}
&X_1 = 2\sqrt[3]{\mathcal{R}}\cos\theta, \quad X_2 = 2\sqrt[3]{\mathcal{R}}\cos\left(\frac{2\pi}{3} + \theta\right),\\
&X_3 = 2\sqrt[3]{\mathcal{R}}\cos\left(\frac{4\pi}{3} + \theta\right),
\end{aligned} \tag{9.55}$$

where

$$\mathcal{R} = \sqrt{-\left(\frac{P}{3}\right)^3}, \quad \theta = \frac{1}{3}\arccos\left(-\frac{Q}{2\mathcal{R}}\right).$$

To solve (9.52), set $\mathcal{Z} = X - \frac{B}{3}$. Then (9.52) is converted into (9.53) with (cf. Exercise 9.6)

$$P = -\frac{B^2}{3} + C, \quad Q = \frac{2B^3}{27} - \frac{BC}{3} + D.$$

Thus the roots of (9.52) are

$$\mathcal{Z}_1 = X_1 - \frac{B}{3}, \quad \mathcal{Z}_2 = X_2 - \frac{B}{3}, \quad \mathcal{Z}_3 = X_3 - \frac{B}{3}. \tag{9.56}$$

If $\mathcal{Z}_1$ is the sole real root, it is selected. In the case where there are three real roots, say,

$$\mathcal{Z}_1 > \mathcal{Z}_2 > \mathcal{Z}_3,$$

we select $\mathcal{Z}_1$ if the vapor (gas) phase dominates. If the liquid (oil) phase dominates, we select $\mathcal{Z}_1$ when $\mathcal{Z}_2 \le 0$; select $\mathcal{Z}_2$ when $\mathcal{Z}_2 > 0$ and $\mathcal{Z}_3 \le 0$; select $\mathcal{Z}_3$ when $\mathcal{Z}_3 > 0$.

9.3.5 Practical considerations

We point out a few practical issues in programming the solution of equilibrium relations.

Iteration switch

As noted, depending on the size of L, different variables, either x_{io} and L or x_{ig} and V, should be used in the flash calculation, $i = 1, 2, \ldots, N_c$. If the gas phase dominates in the hydrocarbon system (e.g., $L < 0.5$), the primary unknowns will be x_{io} and L. If the oil phase dominates (e.g., $L \geq 0.5$), the primary unknowns will be x_{ig} and V. This choice can improve solution accuracy and convergence speed. For example, as L gets close to one, the flash calculation may not converge. In this case, the primary unknown needs to be switched to V. In programming, the switch of iterations should be done automatically.

Determination of bubble points

The following system of $N_c + 1$ equations are solved simultaneously for finding the *bubble point pressure* p and the compositions x_{ig} by an Newton–Raphson iteration ($i = 1, 2, \ldots, N_c$):

$$\begin{aligned} &z_i \varphi_{io}(p, x_{1o}, x_{2o}, \ldots, x_{N_c o}) = x_{ig} \varphi_{ig}(p, x_{1g}, x_{2g}, \ldots, x_{N_c g}), \\ &\sum_{i=1}^{N_c} x_{ig} = 1. \end{aligned} \tag{9.57}$$

In the late steps of the iteration (e.g., after ten iterations), the second equation in (9.57) can be replaced by

$$\sum_{i=1}^{N_c} \frac{\varphi_{io}}{\varphi_{ig}} z_i = 1 \tag{9.58}$$

to speedup convergence. In the Newton–Raphson iteration, if the successive values of pressure change less than a certain value (e.g., 0.01 psi), then this iteration is considered to have converged. We consider that it fails to converge if more than 30 iterations are required or if $|z_i - x_{ig}| < 0.001|z_i|$. In the latter case, the successive substitution method can be used to obtain p and x_{ig}, $i = 1, 2, \ldots, N_c$. A trivial solution occurs when $x_{ig} = z_i$ for any value of p, indicating that a *dew point* occurs.

Determination of dew points

The *dew point pressure* p and the compositions x_{io} satisfy the system of $N_c + 1$ equations ($i = 1, 2, \ldots, N_c$):

$$\begin{aligned} &x_{io} \varphi_{io}(p, x_{1o}, x_{2o}, \ldots, x_{N_c o}) = z_i \varphi_{ig}(p, x_{1g}, x_{2g}, \ldots, x_{N_c g}), \\ &\sum_{i=1}^{N_c} x_{io} = 1. \end{aligned} \tag{9.59}$$

Again, after about ten Newton–Raphson's iterations, the second equation in (9.59) is replaced by

$$\sum_{i=1}^{N_c} \frac{\varphi_{ig}}{\varphi_{io}} z_i = 1. \tag{9.60}$$

Table 9.1. *Reservoir grid data.*

$Nx_1 = Nx_2 = 9$, $Nx_3 = 4$; $h_1 = h_2 = 293.3$ ft
$h_3 = 30, 30, 50, 50$ ft; Datum=7,500 ft. (subsurface)
Porosity: 0.13 (at initial reservoir pressure)
Gas-water contact: 7,500 ft; S_w at contact: 1.0
p_{cgw} at contact: 0.0 psi; initial pressure at contact: 3,550 psia
Water density at contact: 63.0 lb/ft^3; c_w=3.0E-6 psi^{-1}
Formation water viscosity: 0.78 cp; Rock comp.: 4.0E-6 psi^{-1}

Table 9.2. *Reservoir model description.*

Layer	Thickness (ft)	k_h (md)	k_v (md)	Depth to center (ft)
1	30	130	13	7,330
2	30	40	4	7,360
3	50	20	2	7,400
4	50	150	15	7,450

Using the same guidelines as in the treatment of bubble points, if the successive values of pressure in the iteration process change less than 0.01 psi, this iteration is considered to have converged. We consider that the convergence fails if more than 30 iterations are required or if $|z_i - x_{io}| < 0.001|z_i|$. In the latter case, the successive substitution method can be used to obtain p and x_{io}, $i = 1, 2, \ldots, N_c$. A trivial solution occurs when $x_{io} = z_i$ for any value of p, indicating that a *bubble point* occurs.

9.4 The Third SPE Project: Compositional Flow

The simulation problem is chosen from the benchmark problem of the third CSP (Kenyon and Behie, 1987). Nine companies participated in this comparative project. It is a study of gas cycling in a rich retrograte condensate reservoir. Two prediction cases are considered. The first case is gas cycling with constant sales gas removal, and the second case is cycling with some gas sales deferral to enhance pressure maintenance in the early life of the reservoir. The specification of the reservoir model is presented in Tables 9.1–9.5, where k_h ($= k_{11} = k_{22}$) and k_v ($= k_{33}$) denote the horizontal and vertical permeabilities, respectively. A reservoir grid with $9 \times 9 \times 4$ is shown in Figure 9.1, and it is diagonally symmetrical, indicating that it would be possible to simulate half of this reservoir. We chose to model the full reservoir. Also, the reservoir layers are homogeneous and have a constant porosity, but there are permeability and thickness variations between layers, a factor leading to unequal sweepout. The two-well pattern is arbitrary and is employed to allow for some retrograde condensation without significant revaporization by recycling gas to simulate what occurs in sweep-inaccessable parts of a real reservoir.

The CVFE method with linear elements introduced in Section 4.3 is used for the discretization of the governing equations for the compositional model. Due to the layer structure in the vertical direction of the reservoir under consideration, we divide its domain into hexagonal prisms, i.e., hexagons in the horizontal plane and rectangles in the vertical

Table 9.3. *Production, injection, and sales data.*

Production	Location: $i = j = 7$; perforations: $k = 3, 4$; radius = 1 ft; rate: 6,200 MSCF/D (gas rate); min p_{bh}, 500 psi
Injection	Location: $i = j = 1$; perforations: $k = 1, 2$; radius = 1 ft; rate: separator rate-sales rate; max p_{bh}: 4,000 psi
Sales rate for case 1	Constant sales rate to blowdown: $0 < t < 10$ yr, 1,500 MSCF/D; $t > 10$ yr, all produced gas to sales
Sales rate for case 2	Deferred sales: $0 < t < 5$ yr, 500 MSCF/D; $5 < t < 10$ yr, 2,500 MSCF/D; $t > 10$ yr, all produced gas to sales

Table 9.4. *Saturation function data.*

Phase saturation	k_{rg}	k_{ro}	k_{rw}	p_{cgw} (psi)	p_{cgo} (psi)
0.00	0.00	0.00	0.00	> 50	0
0.04	0.005	0.00	0.00	> 50	0
0.08	0.013	0.00	0.00	> 50	0
0.12	0.026	0.00	0.00	> 50	0
0.16	0.040	0.00	0.00	50	0
0.20	0.058	0.00	0.002	32	0
0.24	0.078	0.00	0.010	21	0
0.28	0.100	0.005	0.020	15.5	0
0.32	0.126	0.012	0.033	12.0	0
0.36	0.156	0.024	0.049	9.2	0
0.40	0.187	0.040	0.066	7.0	0
0.44	0.222	0.060	0.090	5.3	0
0.48	0.260	0.082	0.119	4.2	0
0.52	0.300	0.112	0.150	3.4	0
0.56	0.348	0.150	0.186	2.7	0
0.60	0.400	0.196	0.227	2.1	0
0.64	0.450	0.250	0.277	1.7	0
0.68	0.505	0.315	0.330	1.3	0
0.72	0.562	0.400	0.390	1.0	0
0.76	0.620	0.513	0.462	0.7	0
0.80	0.680	0.650	0.540	0.5	0
0.84	0.740	0.800	0.620	0.4	0
0.88	—	—	0.710	0.3	0
0.92	—	—	0.800	0.2	0
0.96	—	—	0.900	0.1	0
1.00	—	—	1.000	0.0	0

Table 9.5. *Separator pressures and temperatures.*

Separator	Pressure (psia)	Temperature (°F)
Primary*	815	80
Primary	315	80
Second stage	65	80
Stock tank	14.7	60

*Primary separation at 815 psia until reservoir pressure (at datum) falls below 2,500 psia; then switch to primary separation at 315 psia.

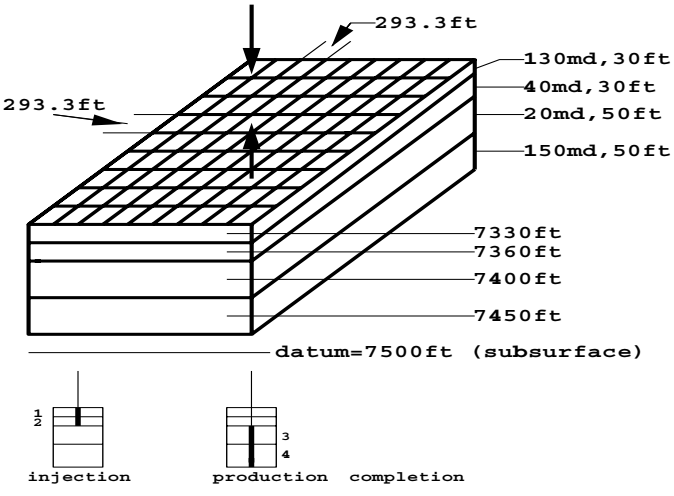

Figure 9.1. *A reservoir domain.*

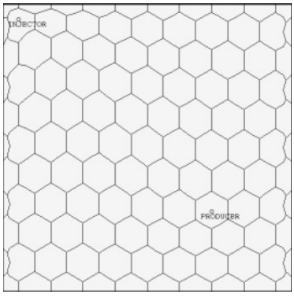

Figure 9.2. *A planar view of the grid.*

direction, as seen in Figure 4.36; also see Figure 9.2 for a planar view of the grid. The initial conditions, the location of the gas-water contact, and the capillary pressure data produce a water-gas transition zone extending to the pay zones. However, the very small compressibility and water volume make water quite insignificant for the present problem. Relative permeability data are used under the assumption that the phase relative permeability function depends only on its own phase saturation. Oil is immobile to 24% saturation, and k_{rg} is reduced from 0.74 to 0.4 as condensate builds to this saturation with irreducible water present.

Production is separator gas rate controlled. Liquid production through multistage separation is to be predicted. The separator train is given, and the primary separator pressure depends on reservoir pressure as shown in Table 9.5. Sales gas is removed from the bulked separator gas, and the remaining gas is recycled. Volumetrically, the two cases under consideration provide for exactly the same amount of recycling gas to be reinjected over the cycling period (10 years), but more gas is recycled in the critical early years in the second case. Blowdown (all gas to sales) starts at the end of the tenth year of cycling, and simulations are run up to 15 years or 1,000 psi average reservoir pressure, whichever occurs

Table 9.6. *Mole fractions of the reservoir fluids.*

Component	Mol percent
Carbon dioxide (CO_2)	1.21
Nitrogen (N_2)	1.94
Methane (C_1)	65.99
Ethane (C_2)	8.69
Propane (C_3)	5.91
Iso-butane (IC_4)	2.39
N-butane (NC_4)	2.78
Iso-pentane (IC_5)	1.57
N-pentane (NC_5)	1.12
Hexanes (C_6)	1.81
Heptanes plus (C_{7+})*	6.59

*Properties of heptanes plus: specific gravity at 60°F = 0.774;
API gravity at 60°F = 51.4; molecular weight=140.
Computed separator gas gravity (air=1.0)=0.736.
Computed gross heating value for separator gas=1,216 Btu
per cubic foot of dry gas at 14.65 psia and 60°F.
Primary separator gas/separator liquid ratio
=4,812 SCF/bbl at 72°F and 2,000 psig.

Table 9.7. *Pressure volume relations of reservoir fluid at* 200° *F.*

Pressure (psig)	Relative volume	Deviation factor Z
6,000	0.8045	1.129
5,500	0.8268	1.063
5,000	0.8530	0.998
4,500	0.8856	0.933
4,000	0.9284	0.869
3,600	0.9745	0.822
3,428 (dew point)	1.0000	0.803*
3,400	1.0043	
3,350	1.0142	
3,200	1.0468	
3,000	1.0997	
2,800	1.1644	
2,400	1.3412	
2,000	1.6113	
1,600	2.0412	
1,300	2.5542	
1,030	3.2925	
836	4.1393	

*Gas expansion factor=1.295 MSCF/bbl.

first. The simulations are initialized at pressure about 100 psi above the dew point pressure 3,443 psia.

The entire compositional simulation study is divided into two steps:

- A PVT phase behavior study to obtain accurate EOS parameters and prediction results.
- A reservoir simulation study of the compositional flow using the CVFE.

Table 9.8. *Hydrocarbon analysis of lean gas sample.*

Component*	Mol percent	GPM
Hydrogen sulfids	Nil	
Carbon dioxide (CO_2)	Nil	
Nitrogen (N_2)	Nil	
Methane (C_1)	94.69	
Ethane (C_2)	5.27	1.401
Propane (C_3)	0.05	0.014
Butanes plus (C_{4+})	Nil	
Total	100.00	1.415

*Computed gas gravity (air=1.0)=0.58.
Computed gross heating value =1,216 Btu
per cubic foot of dry gas at 14.65 psia and 60°F.

Table 9.9. *Pressure volume relations of mixture No.* 1 *at* 200° *F.*

Pressure (psig)	Relative volume*	Liquid volume (percent of saturated volume)
6,000	0.9115	
5,502	0.9387	
5,000	0.9719	
4,500	1.0135	
4,000	1.0687	
3,800	1.0965	
3,700	1.1116	
3,650	1.1203	
3,635 (dew point)	1.1224	0.0
3,600	1.1298	0.3
3,500	1.1508	1.7
3,300	1.1969	6.8
3,000	1.2918	12.8

*Relative volumes and liquid volume percents are all based on original hydrocarbon pore volume at 3,428 psig and 200°F.

Table 9.10. *Pressure volume relations of mixture No.* 2 *at* 200° *F.*

Pressure (psig)	Relative volume	Liquid volume (percent of saturated volume)
6,000	1.1294	
5,500	1.1686	
5,000	1.2162	
4,500	1.2767	
4,300	1.3064	
4,100	1.3385	
4,050	1.3479	
4,015 (dew point)	1.3542	0.0
3,950	1.3667	0.1
3,800	1.3992	0.5
3,400	1.5115	4.5
3,000	1.6709	9.4

Table 9.11. *Pressure volume relations of mixture No.* 3 *at* 200° *F.*

Pressure (psig)	Relative volume	Liquid volume (percent of saturated volume)
6,000	1.6865	
5,600	1.7413	
5,300	1.7884	
5,100	1.8233	
5,000	1.8422	
4,950	1.8519	
4,900	1.8620	
4,800	1.8827	
4,700	1.9043	
4,610 (dew point)	1.9248	
4,500	1.9512	0.1
4,200	2.0360	0.3
3,900	2.1378	0.6
3,500	2.3193	2.1
3,000	2.6348	6.0

Table 9.12. *Pressure volume relations of mixture No.* 4 *at* 200° *F.*

Pressure (psig)	Relative volume	Liquid volume (percent of saturated volume)
6,000	2.2435	
5,500	2.3454	
5,000	2.4704	
4,880 (dew point)	2.5043	0.0
4,800	2.5288	Trace
4,600	2.5946	0.1
4,400	2.6709	0.3
4,000	2.8478	0.7
3,500	3.1570	1.4
3,000	3.5976	3.6

9.4.1 PVT phase behavior study

PVT data

The measured PVT data are shown in Tables 9.6–9.16. These data include hydrocarbon sample analysis, constant composition expansion data, constant volume depletion data, and swelling data of four mixtures of reservoir gas with lean gas. Table 9.6 gives the mole fractions of the reservoir fluids. Table 9.7 describes the constant composition expansion data, and the computed Z-factors at and above the dew point pressure. Tables 9.8–9.12 show data for the swelling tests of reservoir gas with lean gas. Table 9.8 gives the lean gas composition. Note that it is virtually free of C_{3+} fractions. This contrasts with the separator gas recycled in the reservoir problem, which has about 10% of C_{3+}. Hence matching the swelling data is more significant for recycling with gas plant residue gas than for typical separator gas compositions. Tables 9.9–9.12 indicate the pressure-volume data for expansions at 200° F for four mixtures (with the respective mole fractions: 0.1271, 0.3046, 0.5384, and 0.6538)

Table 9.13. *Retrograde condensation during gas depletion at* 200° *F.*

Pressure (psig)	Retrograde liquid volume (percent of hydrocarbon pore space)
3,428 (dew point)	0.0
3,400	0.9
3,350	2.7
3,200	8.1
3,000 (first depletion level)	15.0
2,400	19.9
1,800	19.2
1,200	17.1
700	15.2
0	10.2

Table 9.14. *Computed cumulative recovery during depletion.*

		Reservoir pressure (psig)					
Cumulative recovery per MMSCF of original fluid	Initial in place	3,428	3,000	2,400	1,800	1,200	700
Well stream (MSCF)	1,000	0	90.95	247.02	420.26	596.87	740.19
Normal temp. separation* Stock tank liquid (B)	131.00	0	7.35	14.83	20.43	25.14	29.25
Primary separator gas (MSCF)	750.46	0	74.75	211.89	369.22	530.64	666.19
Second stage gas (MSCF)	107.05	0	7.25	16.07	23.76	31.45	32.92
Stock tank gas (MSCF)	27.25	0	2.02	4.70	7.15	9.69	11.67
Total "plant products" in primary separator sas (Gallons)							
Propane (C_3)	801	0	85	249	443	654	876
Butanes (total C_4)	492	0	54	613	295	440	617
Pentanes plus (C_{5+})	206	0	22	67	120	176	255
Total "plant products" in 2nd stage gas (gallons)							
Propane (C_3)	496	0	35	80	119	161	168
Butanes (total C_4)	394	0	30	69	106	146	153
Pentanes plus (C_{5+})	164	0	12	29	45	62	65
Total plant products in well stream (gallons)							
Propane (C_3)	1,617	0	141	374	629	900	1,146
Butanes (total C_4)	1,648	0	137	352	580	821	1,049
Pentanes plus (C_{5+})	5,464	0	321	678	973	1,240	1,488

*Primary separator at 800 psig and 80° F reduced to 300 psig and 80° F for reservoir pressure below 1,200 psig; second stage at 50 psig and 80° F; stock tonk at 0 psig and 60° F.

of lean gas with reservoir gas. Liquid dropout data are shown for each of the expansions. Table 9.13 gives retrograde condensation during gas depletion (constant volume depletion) of the original reservoir fluids. Table 9.14 indicates the computed yields of separator and gas plant products, and Table 9.15 shows compositions of equilibrium gas during constant volume depletion. We use these data to match the surface volumes generated by reservoir gas processed in the multistage separators. Table 9.16 gives the results of the swelling

Table 9.15. *Hydrocarbon analysis of produced well stream-Mol percent: Depletion study at* 200° *F.*

	Reservoir pressure (psig)						
Component	3,428	3,000	2,400	1,800	1,200	700	700*
Carbon dioxide (CO_2)	1.21	1.24	1.27	1.31	1.33	1.32	0.44
Nitrogen (N_2)	1.94	2.13	2.24	2.27	2.20	2.03	0.14
Methane (C_1)	65.99	69.78	72.72	73.98	73.68	71.36	12.80
Ethane (C_2)	8.69	8.66	8.63	8.79	9.12	9.66	5.27
Propane (C_3)	5.91	5.67	5.46	5.38	5.61	6.27	7.12
Iso-butane (IC_4)	2.39	2.20	2.01	1.93	2.01	2.40	4.44
N-butane (NC_4)	2.78	2.54	2.31	2.18	2.27	2.60	5.96
Iso-pentane (IC_5)	1.57	1.39	1.20	1.09	1.09	1.23	4.76
N-pentane (NC_5)	1.12	0.96	0.82	0.73	0.72	0.84	3.74
Hexanes (C_6)	1.81	1.43	1.08	0.88	0.83	1.02	8.46
Heptanes (C_7)	1.44	1.06	0.73	0.55	0.49	0.60	8.09
Octanes (C_8)	1.50	1.06	0.66	0.44	0.34	0.40	9.72
Nonanes (C_9)	1.05	0.69	0.40	0.25	0.18	0.16	7.46
Decanes (C_{10})	0.73	0.43	0.22	0.12	0.08	0.07	5.58
Undecanes (C_{11})	0.49	0.26	0.12	0.06	0.03	0.02	3.96
Dodecanes plus (C_{12+})	1.38	0.50	0.13	0.04	0.02	0.02	12.06
Total	100.00	100.00	100.00	100.00	100.00	100.00	100.00
Molecular weight of heptanes plus (C_{7+})	140	127	118	111	106	105	148
Specific gravity of heptanes plus (C_{7+})	0.774	0.761	0.752	0.745	0.740	0.739	0.781
Deviation Z-factor Equilibrium gas	0.803	0.798	0.802	0.830	0.877	0.924	
Two phase	0.803	0.774	0.748	0.730	0.703	0.642	
Well stream produced-Cumulative percent of initial	0.00	9.095	24.702	42.026	59.687	74.019	
GPM from smooth compositions Propane plus (C_{3+})	8.729	6.598	5.159	4.485	4.407	5.043	
Butanes plus (C_{4+})	7.112	5.046	3.665	3.013	2.872	3.328	
Pentanes plus (C_{5+})	5.464	3.535	2.287	1.702	1.507	1.732	

*Equilibrium liquid phase, representing 10.762% of original well stream.

Table 9.16. *Solubility and swelling test at* 200° *F (injection gas-lean gas).*

Mixture number	Cumul. gas injected (SCF/bbl)(1)	Cumul. gas injected (Mol fraction)(2)	Swollen volume(3)	Dew point pressure (psig)
0*	0.0	0.0000	1.0000	3,428
1	190	0.1271	1.1224	3,635
2	572	0.3046	1.3542	4,015
3	1,523	0.5384	1.9248	4,610
4	2,467	0.6538	2.5043	4,880

*Original reservoir fluid.
(1) SCF/bbl is the cumulative cubic feet of injection gas at 14.65 psia and 60° F per barrel of original reservoir fluid at 3,428 psig and 200° F.
(2) Mol fraction is cumulative mols of injection gas per total mols of indicated mixture.
(3) Swollen volume is barrels of indicated mixture at its dew point pressure and 200° F per barrel of original reservoir fluid at 3,428 psig and 200° F.

Table 9.17. HC_1, HC_2, *and* HC_3.

Component	Mole fraction	Molecular weights	Specific gravity
HC_1	0.05011	118.44	0.74985
HC_2	0.01340	193.95	0.81023
HC_3	0.00238	295.30	0.86651

Table 9.18. *Pseudogrouping of components.*

Pseudocomponent	P_1	P_2	P_3	P_4	P_5	P_6	P_7
Natural component	C_1, N_2	C_2, CO_2	C_3, C_4	C_5, C_6	HC_1	HC_2	HC_3
Mole fraction	0.6793	0.0990	0.1108	0.0450	0.05011	0.0134	0.00238
Molecular weights	16.38	31.77	50.64	77.78	118.44	193.95	295.30

experiments of reservoir gas with lean gas for the four samples. Note that the dew point pressure increases by approximately 50% for lean gas additions of 2,467 SCF/bbl for a total gas content of about 8,000–9,000 SCF/STB.

PVT study for matching the PVT data

The PVT study includes:

- splitting C_{7+},
- pseudogrouping,
- constant composition expansion and constant volume depletion,
- swelling tests,
- critical parameters at the formation and separator conditions for compositional modeling.

The heavy C_{7+} component is split into three components, HC_1, HC_2, and HC_3, to enhance the accuracy of PVT data matching. The mole fractions, molecular weights, and specific gravity of these components are stated in Table 9.17.

We use a pseudogrouping approach to group components. The purpose of pseudogrouping is to reduce the number of components involved in compositional modeling. These pseudocomponents are described in Table 9.18.

Detailed matches of the PVT data are displayed in Figures 9.3–9.6. Figure 9.3 shows pressure-volume data in constant composition expansion of the reservoir gas at 200° F. Figure 9.4 indicates retrograde condensate during constant volume depletion. Liquid yield by multistage surface separation in reservoir gas produced by constant volume depletion is displayed in Figure 9.5. The results of swelling of reservoir gas with increasing the dew point pressure of injected lean gas are given in Figure 9.6. There is a very good agreement between the laboratory and computed PVT data.

Finally, Tables 9.19–9.22 give a summary for the characterization data and binary interaction coefficients of the components at the formation and separator conditions.

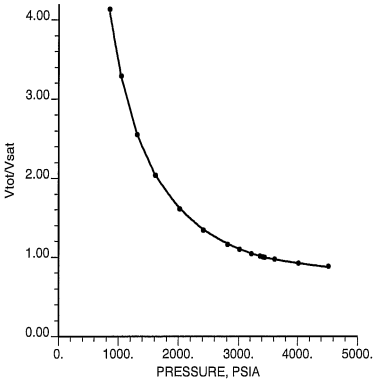

Figure 9.3. *Pressure-volume relation of reservoir fluid at* 200° *F: Constant composition expansion (cf. Table* 9.7*); laboratory data (dotted) and computed data (solid).*

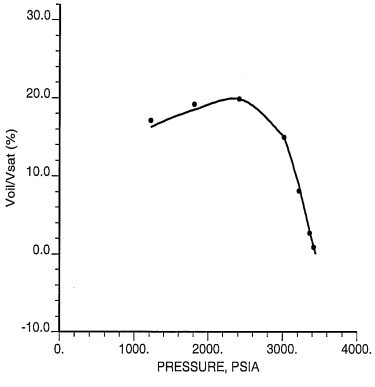

Figure 9.4. *Retrograde condensate during constant volume gas depletion at* 200° *F (cf. Table* 9.13*); laboratory data (dotted) and computed data (solid).*

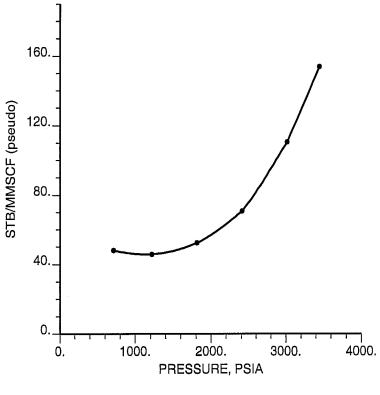

Figure 9.5. *Three-stage separator yield during constant volume gas depletion at* 200° *F (cf. Table* 9.14*); laboratory data (dotted) and computed data (solid).*

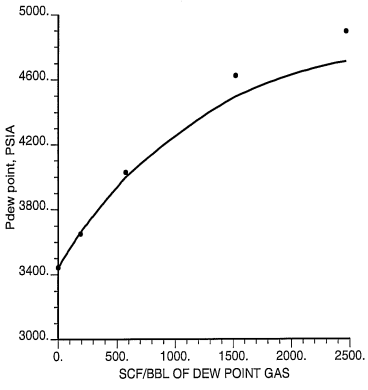

Figure 9.6. *Dew point pressure versus cumulative gas injected during swelling with lean gas at* 200° *F (cf. Table* 9.16*); laboratory data (dotted) and computed data (solid).*

Table 9.19. *Characterization data of components at the formation conditions.*

Pseudo-components	Z_c	P_c (psia)	T_c (°F)	Molecular weight	Acentric ω	Ω_a	Ω_b
P_1	0.28968	667.96	−119.11	16.38	0.00891	0.34477208	0.06328161
P_2	0.28385	753.82	90.01	31.77	0.11352	0.52197368	0.09982480
P_3	0.27532	586.26	252.71	50.64	0.17113	0.51497212	0.10747888
P_4	0.26699	469.59	413.50	77.78	0.26910	0.41916871	0.09345540
P_5	0.27164	410.14	605.99	118.44	0.34196	0.48594317	0.07486045
P_6	0.23907	260.33	795.11	193.95	0.51730	0.57058309	0.10120595
P_7	0.22216	183.92	988.26	295.30	0.72755	0.45723552	0.07779607

Table 9.20. *Binary interaction coefficients at the formation conditions.*

Components	P_1	P_2	P_3	P_4	P_5	P_6	P_7
P_1	0.0						
P_2	0.000622	0.0					
P_3	−0.002471	−0.001540	0.0				
P_4	0.011418	0.010046	0.002246	0.0			
P_5	−0.028367	0.010046	0.002246	0.0	0.0		
P_6	−0.100000	0.010046	0.002246	0.0	0.0	0.0	
P_7	0.206868	0.010046	0.002246	0.0	0.0	0.0	0.0

Table 9.21. *Characterization data of components at the separator conditions.*

Pseudo-components	Z_c	P_c (psia)	T_c (°F)	Molecular weight	Acentric ω	Ω_a	Ω_b
P_1	0.28968	667.96	−119.11	16.38	0.00891	0.50202385	0.09960379
P_2	0.28385	753.82	90.01	31.77	0.11352	0.45532152	0.08975547
P_3	0.27532	586.26	252.71	50.64	0.17113	0.46923415	0.08221724
P_4	0.26699	469.59	413.50	77.78	0.26910	0.58758251	0.08178213
P_5	0.27164	410.14	605.99	118.44	0.34196	0.55567652	0.06715680
P_6	0.23907	260.33	795.11	193.95	0.51730	0.49997263	0.07695341
P_7	0.22216	183.92	988.26	295.30	0.72755	0.45723552	0.07779607

Table 9.22. *Binary interaction coefficients at the separator conditions.*

Components	P_1	P_2	P_3	P_4	P_5	P_6	P_7
P_1	0.0						
P_2	0.000622	0.0					
P_3	−0.002471	−0.001540	0.0				
P_4	0.011418	0.010046	0.002246	0.0			
P_5	0.117508	0.010046	0.002246	0.0	0.0		
P_6	0.149871	0.010046	0.002246	0.0	0.0	0.0	
P_7	0.112452	0.010046	0.002246	0.0	0.0	0.0	0.0

Table 9.23. *The initial fluids in-place.*

Wet gas (BSCF)	Dry gas (BSCF)	Stock tank oil (MMSTB)
25.774	23.246	3.450

9.4.2 Reservoir simulation study

The initial fluids in-place using multistage separation are given in Table 9.23. Simulation results for the compositional model considered are given in Figures 9.7–9.13. The time step size used in iterative IMPES is about 30 days (in the first few time steps, it is smaller). The compositional simulator uses the ORTHOMIN Krylov subspace algorithm, with incomplete LU factorization preconditioners (cf. Chapter 5), as the linear solver.

As noted earlier, the first case is gas cycling with constant sales gas removal, while the second case is cycling with some gas sales deferral to enhance pressure maintenance in the early life of the reservoir. The total sales gas removal is the same for the two cases; the difference lies in the way sales gas is removed in the first ten years (cf. Table 9.3). For a gas condensate reservoir, decreasing the occurrence of retrograde condensate phenomena leads to less loss of heavy hydrocarbon components and more production of oil.

Stock-tank oil rates for the first and second cases and the corresponding cumulative liquid production for these cases at the final simulation time of 15 years are shown in Figures 9.7–9.10. Incremental stock-tank oil produced by gas-sales deferral (the second case minus the first), and oil saturations are given in Figures 9.11–9.13. Primary separator switchout occurs late in the cycling phase (10 years). The predicted surface oil rate is closely correlated with the liquid yield predictions shown in Figure 9.5.

Figure 9.11 gives the incremental stock-tank oil produced by gas-sales deferral. At the peak of this curve (at the eighth year), the cumulative stock-tank oil produced by the second case is 182 MSTB more than that from the first case (i.e, 9.76% increase). At the final production time (the 15th year), the increase is down to 159 MSTB (6.65%). This phenomenon can be understood from the observation that after injection of recycle gas stops, liquid production is due to depletion only, and the heavy end fractions vaporize into the vapor phase and are produced.

Figures 9.12 and 9.13 give the oil saturation at the gridblock (7,7,4) for these two cases, respectively. From these two figures, we see that the oil saturation in the second case is smaller than that in the first case. This shows that the retrograde condensate phenomenon in the second case occurs less than that in the first.

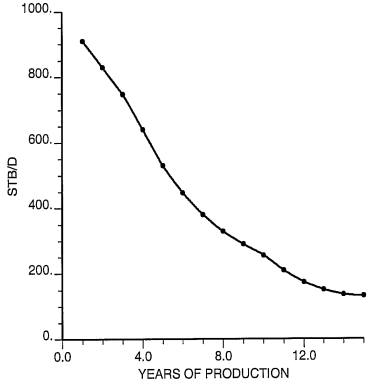

Figure 9.7. *Stock-tank oil production rate in case* 1.

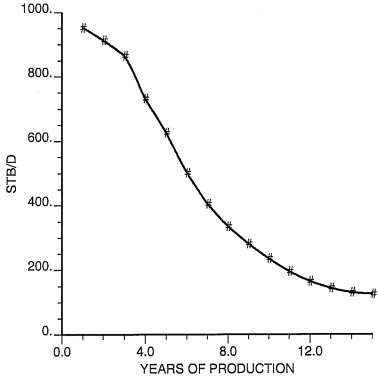

Figure 9.8. *Stock-tank oil production rate in case* 2.

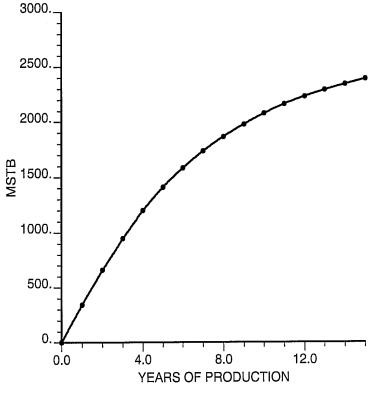

Figure 9.9. *Cumulative stock-tank oil production in case* 1.

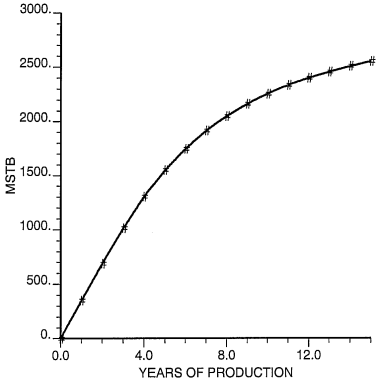

Figure 9.10. *Cumulative stock-tank oil production in case* 2.

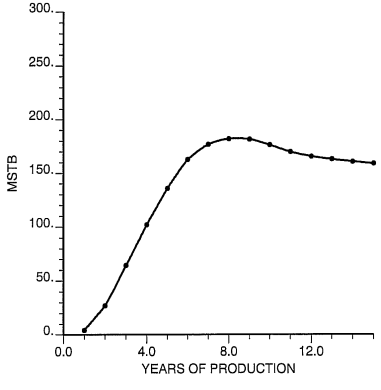

Figure 9.11. *Incremental stock-tank oil produced by gas-sales deferral (case* 2 *minus case* 1*).*

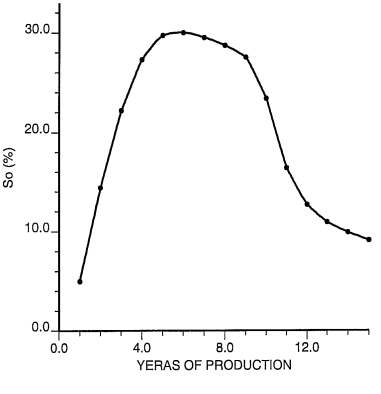

Figure 9.12. *Oil saturation in grid block* (7,7,4) *in case* 1.

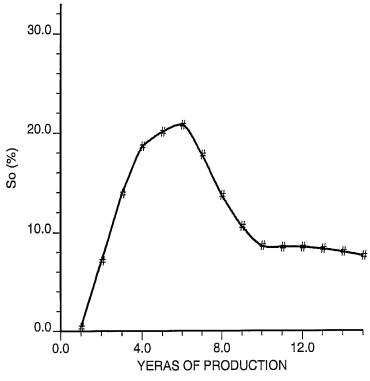

Figure 9.13. *Oil saturation in grid block* (7,7,4) *in case* 2.

Compared with those prepared by the nine companies (Kenyon and Behie, 1987), the numerical results in Figures 9.7–9.13 show that the numerical scheme here performs very well. The stock-tank oil rate and corresponding cumulative production are close to the respective averaged values of those provided by nine companies (Kenyon and Behie, 1987). In the numerical scheme for the compositional simulation here, the treatment of crossing "bubble points" and "dew points" in a Newton–Raphson iteration is very accurate, which leads to a very accurate computation of Jacobian matrices when the flow changes from three-phase to two-phase or vice versa. The scheme here also utilizes an accurate postprocessing technique for checking consistency of the solution variables (F, L) with the natural variables (S_o, S_g) after the Newton–Raphson iteration.

9.4.3 Computational remarks

We have applied an iterative IMPES solution technique to the numerical simulation of three-dimensional, three-phase, multicomponent compositional flow in porous media. The CVFE method with linear elements was employed for discretizing the governing equations of this compositional model. Numerical experiments were presented for the benchmark problem of the third CSP and showed that the iterative IMPES technique performs very well for this problem of a moderate size. To simulate accurately the process of recycle gas injection in a gas condensate reservoir using a compositional model, from our experience the following factors are very important:

- Through a PVT data match of the retrograde condensate curve during constant volume depletion, one can predict accurately the change of the reservoir oil saturation during a pressure decrease.

- Through a PVT data match of swelling tests, one sees that the increase of the dew point pressure after injection of recycle gas can lead to the transfer of heavy hydrocarbon components in the thermodynamic equilibrium from the liquid phase to the vapor phase and to the production of these components at production wells, thus increasing production.

- In compositional simulations, it is necessary to input two sets of critical PVT data; one for high pressure used for simulation of a reservoir flow process, and the other for lower pressure used for simulation of a separator process. The efficiency of enhanced oil recovery depends on the accuracy of the separator simulation.

The simulations in this section were performed on an SGI Power Indigo with 1 GB RAM, and the CPU time for the present compositional problem at the final time of 15 years is about 39 seconds.

9.5 Bibliographical Remarks

The choice of primary variables made in Section 9.2.1 follows Nolen (1973) and Young and Stephenson (1983). The numerical results reported in Section 9.4 are taken from Chen et al. (2005A), which contains additional numerical results. More information about the data used in the third SPE CSP can be found in Kenyon and Behie (1987).

Exercises

9.1. Derive equation (9.22) using the second equation in (9.3) and equations (9.4), (9.16), and (9.21) and neglecting the variation of ρ_α with respect to space.

9.2. For the Newton–Raphson flash calculation introduced in Section 9.3.2, evaluate $\partial\varphi_{i\alpha}/\partial x_{j\alpha}$, $i, j = 1, 2, \ldots, N_c$, $\alpha = o, g$.

9.3. For the Newton–Raphson flash calculation introduced in Section 9.3.2, compute $\partial Z_\alpha/\partial x_{j\alpha}$, $j = 1, 2, \ldots, N_c$, $\alpha = o, g$.

9.4. Given the cubic equation

$$X^3 + PX + Q = 0,$$

show that its three roots are

$$X_1 = \sqrt[3]{-\frac{Q}{2} + \sqrt{\left(\frac{Q}{2}\right)^2 + \left(\frac{P}{3}\right)^3}} + \sqrt[3]{-\frac{Q}{2} - \sqrt{\left(\frac{Q}{2}\right)^2 + \left(\frac{P}{3}\right)^3}},$$

$$X_2 = \omega \sqrt[3]{-\frac{Q}{2} + \sqrt{\left(\frac{Q}{2}\right)^2 + \left(\frac{P}{3}\right)^3}} + \omega^2 \sqrt[3]{-\frac{Q}{2} - \sqrt{\left(\frac{Q}{2}\right)^2 + \left(\frac{P}{3}\right)^3}},$$

$$X_3 = \omega^2 \sqrt[3]{-\frac{Q}{2} + \sqrt{\left(\frac{Q}{2}\right)^2 + \left(\frac{P}{3}\right)^3}} + \omega \sqrt[3]{-\frac{Q}{2} - \sqrt{\left(\frac{Q}{2}\right)^2 + \left(\frac{P}{3}\right)^3}}.$$

9.5. Let X_1, X_2, and X_3 be the three roots in Exercise 9.4. Prove that they satisfy equations (9.54).

9.6. Defining $\mathcal{Z} = X - \frac{B}{3}$, show that equation (9.52) can be transformed into equation (9.53) with

$$P = -\frac{B^2}{3} + C, \quad Q = \frac{2B^3}{27} - \frac{BC}{3} + D.$$

9.7. Prove that the three roots $\mathcal{Z}_1$, $\mathcal{Z}_2$, and $\mathcal{Z}_3$ of equation (9.52) satisfy

$$\mathcal{Z}_1 + \mathcal{Z}_2 + \mathcal{Z}_3 = -B, \quad \frac{1}{\mathcal{Z}_1} + \frac{1}{\mathcal{Z}_2} + \frac{1}{\mathcal{Z}_3} = -\frac{C}{D}, \quad \mathcal{Z}_1\mathcal{Z}_2\mathcal{Z}_3 = -D.$$